

Effects of thermal annealing on structural and electrical properties of surface-activated n-GaSb/n-GaInP direct wafer bonds

Felix Predan,^{1,a)} András Kovács,² Jens Ohlmann,¹ David Lackner,¹
 Rafal E. Dunin-Borkowski,² Frank Dimroth,¹ and Wolfgang Jäger³

¹Fraunhofer Institute for Solar Energy Systems ISE, Heidenhofstraße 2, 79110 Freiburg, Germany

²Ernst Ruska-Centre for Microscopy and Spectroscopy with Electrons, Peter Grünberg Institute, Forschungszentrum Jülich, 52425 Jülich, Germany

³Institute for Materials Science, Christian-Albrechts-University of Kiel, Kaiserstrasse 2, 24143 Kiel, Germany

(Received 11 May 2017; accepted 28 August 2017; published online 4 October 2017)

A study on the microstructure of argon-beam activated n-GaSb/n-Ga_{0.32}In_{0.68}P bond interfaces is presented, focusing on the behavior of the bond upon thermal annealing and the relationship with electrical bond properties. Structural investigations of annealed samples utilizing high-resolution transmission electron microscopy combined with energy dispersive x-ray spectroscopy are discussed and compared with electrical current-voltage measurements. An amorphous interlayer of ~ 1.4 nm thickness between the n-GaSb and n-Ga_{0.32}In_{0.68}P originates from the argon sputtering process. This layer continuously recrystallizes upon thermal annealing, creating a mostly crystalline interface at an annealing temperature of 500 °C. Additionally at 400 °C, In enrichment is observed in the near-surface regions of GaSb and pores are generated at the interface. At 500 °C, larger pores are observed and the In enrichment continues, leading to the formation of crystalline In precipitates within the GaSb crystal. The observed changes in the interfacial microstructure upon annealing correlate with variations in the electrical bond resistances. All bonds show ohmic *IV*-characteristics with resistances in the range of few m Ω cm². However, the bond resistance decreases after annealing at temperatures up to 350 °C but increases after annealing at higher temperatures. This behaviour agrees with the observation of reduced amorphous layer thickness upon annealing and with the formation of new induced interfacial defects for annealing temperatures above 350 °C. © 2017 Author(s). All article content, except where otherwise noted, is licensed under a Creative Commons Attribution (CC BY) license (<http://creativecommons.org/licenses/by/4.0/>). [<http://dx.doi.org/10.1063/1.5002080>]

I. INTRODUCTION

III-V compound semiconductors offer a wide range of unique material properties, such as high carrier mobility and absorption coefficient, as well as tunable bandgaps from 2.5 eV down to 0.1 eV.¹ In multi-junction solar cells, compound semiconductors with decreasing bandgaps are stacked on top of each other to successively absorb the solar spectrum. Today, the highest conversion efficiency of 46.0% is achieved with a four-junction device, combining III-V materials grown on InP and GaAs substrates.² This solar cell is enabled by a direct wafer bond to overcome the difference in the lattice constant of 3.6% between InP and GaAs compounds. An alternative approach for a four-junction solar cell concept with prospect of achieving 50% efficiency is based on the materials Ga_{0.50}In_{0.50}P/GaAs/Ga_{0.79}In_{0.21}As//GaSb.³ This cell requires a wafer bond between metamorphic Ga_{0.79}In_{0.21}As and GaSb to overcome a lattice mismatch of 5.9%. Surface-activated bonding (SAB) has been successfully applied to a number of III-V compounds following the original approach of Suga *et al.* for Al/Al and Al/Si₃N₄ wafer bonds.⁴ This technology offers the possibility to monolithically integrate semiconductors with different lattice constants as the resulting bond interfaces are incoherent.⁵ The wafer

bonding process has been shown to be applicable to arsenides,^{6–8} phosphides,^{9,10} and antimonides^{11,12} and capable of achieving both optical transparency and electrical conductivity. We investigate the bonding of n-Ga_{0.32}In_{0.68}P to n-GaSb for the realization of a four-junction solar cell based on GaSb. Here, high electrical conductivity and optical transparency are key requirements.

Transmission electron microscopy has been previously applied to surface-activated bonds, revealing that the atom-beam sputter activation leads to the formation of an amorphous interlayer at the bond interface. Takagi *et al.* showed that the thickness of this amorphous layer for Ar treated Si/Si wafer bonds depends on the induced surface damage or, more specifically, on the kinetic energy of the Ar atoms.¹³ Furthermore, it was reported that the amorphous layer thickness can be reduced by an annealing step up to the point of complete recrystallization.^{13,14} For the widely investigated Si/GaAs wafer bond, the typical amorphous layer thickness is between 2 and 3 nm.^{15–17} Depending on the experimental setup, metallic impurities resulting from the activation process were detected at the bond interface by spectroscopic methods using scanning TEM (STEM).^{16,18} Howlander *et al.* reported initial amorphous layer thicknesses of 7 nm for GaP/GaAs bonds, which were reduced to 6.5 nm after 200 °C annealing and completely absent after an increase in the annealing temperature to 400 and 600 °C.¹⁹ The overall

^{a)}Electronic mail: felix.predan@ise.fraunhofer.de

conductivity vs. voltage behavior was reported to be diode-like in this case; however, the overall resulting electrical conductivity increased for higher annealing temperatures.¹⁹

In this study, we present an analysis of the effects of thermal annealing up to 500 °C on the microstructure and electrical properties of n-GaSb/n-Ga_{0.32}In_{0.68}P wafer bonded interfaces. Several aspects of the bond, such as the dependence of electrical properties on activation parameters, were already reported in Ref. 12. Now, in the presented paper, we correlate the electrical behavior upon annealing with extensive characterization of the bond microstructure using high-resolution Transmission electron microscopy (TEM). Therefore, structural and chemical characterizations by TEM and energy dispersive x-ray spectroscopy (EDXS) are compared to measurements of current-voltage (*I-V*) characteristics of identical n-GaSb/n-Ga_{0.32}In_{0.68}P bond interfaces. The detailed understanding of surface-activated bonds and thermal annealing effects on the atomic scale is of general value for the design of devices that require high electrical conductivity.

II. EXPERIMENTAL

Different bond layers were grown by metalorganic vapor phase epitaxy (MOVPE). 500 nm n-GaSb with a Te doping of nominally $1 \times 10^{18} \text{ cm}^{-3}$ was grown on a 500 μm thick 2 in. n-GaSb wafer with an orientation of (100) 4° towards (111) A. For the n-Ga_{0.32}In_{0.68}P bond layer, a metamorphic Ga_xIn_{1-x}As buffer structure was grown on a 450 μm thick 4 in. n-GaAs wafer oriented (100) 6° off towards (1-11) B to match a lattice constant of 5.73 Å. Then, 500 nm n-Ga_{0.32}In_{0.68}P with Si doping of nominally $1 \times 10^{19} \text{ cm}^{-3}$ was grown lattice-matched to the underlying Ga_xIn_{1-x}As buffer. The bond layers were polished at the company III-V Reclaim in order to reach a low root mean square (RMS) roughness <1 nm, which is essential for a successful and reproducible bonding process.²⁰

The actual bonding process was performed in an Ayumi SAB-100 wafer bonder under ultra-high vacuum conditions at pressures $<3 \times 10^{-6} \text{ Pa}$. The argon atom beam was generated in two saddle field atom-beam sources and applied to the wafer surfaces at an angle of 45°. The kinetic energy of the argon projectiles is typically about 0.4 to 0.6 times the product of the acceleration voltage and the elemental charge. For the experiments, an acceleration voltage of 620 V, an anode current of 50 mA (correlates with the sputtering dose²¹), and a temperature of 120 °C were chosen. The GaSb surface was sputtered for 8 min and the Ga_{0.32}In_{0.68}P surface for 40 s. These durations were chosen to avoid surface wrinkling, which is especially important in the case of Ga_{0.32}In_{0.68}P as this material shows a prominent selective sputtering behavior.¹² After the activation, the semiconductor wafers were pressed together for 5 min at 120 °C with a pressure of 5 MPa, enabling the dangling bonds on the surfaces to form covalent bonds and permanently join the semiconductors.

I-V curves were measured to characterize the electrical conductivity over the bond interface. The investigated wafer bond was cut into two halves and one half was fully metallized on both sides to enable contacting. A Pd/Ge/Au/Ti/Pd/Ag contact was used on the n-GaAs wafer and a Ti/Pd/Au/

Ag contact on the n-GaSb wafer, respectively. Subsequently, the wafer bonds were cut into $3 \times 3 \text{ mm}^2$ pieces and the samples were annealed *ex situ* in forming gas for 1 min at temperatures of 300, 350, 400, and 500 °C. The *I-V* curves were measured using a two-point probe method. The ohmic resistances of the corresponding metal contacts and the substrates were independently measured and subtracted from the *I-V* curves of the metallized wafer bond samples. By doing so, the presented *I-V* characteristics are not influenced by parasitic resistances and the bond resistance per area in Ωcm^2 could be calculated directly from the *I-V* curves with the corresponding sample size of 9 mm^2 .

The microstructures of the bond interfaces and the regions in the vicinity of the interfaces were characterized at high spatial resolution by applying advanced methods of aberration-corrected TEM. For this, the second half of the bonded n-GaSb/n-Ga_{0.32}In_{0.68}P wafer pair was cut into $5 \times 5 \text{ mm}^2$ pieces. Cross-sectional TEM specimens were prepared from samples in the as-bonded state as well as from samples which were annealed at 300, 400, and 500 °C. The annealing was performed *ex situ* for 1 min in a forming gas atmosphere. Conventional mechanical polishing and Ar ion milling at 2.5 keV using a Gatan precision ion polishing system were applied to prepare the electron transparent TEM specimens. The microstructure characterization was performed using high-angle annular dark-field (HAADF) STEM imaging in a probe aberration-corrected FEI Titan microscope operated at 200 kV. The aberrations up to fourth order were corrected with small values, by eliminating resolution limiting aberration effects within the illumination aperture of 25 mrad radius, thus obtaining a probe diameter better than 0.1 nm. The used annular dark-field inner detector semi-angle was 69.1 mrad. Elemental mappings were conducted simultaneously using EDXS in the STEM mode. The line profiles were extracted using the x-ray K lines of elements and quantified by removing the background and applying the Cliff-Lorimer method²² in Bruker Esprit software.

III. RESULTS

Figure 1 shows the *I-V* characteristics of the n-GaSb/n-Ga_{0.32}In_{0.68}P heterojunction after a 1 min annealing treatment at 300, 350, 400, and 500 °C. Ohmic behavior of the carrier transport is observed for every annealing temperature.

Figure 2 shows high-resolution HAADF STEM images of the n-GaSb/n-Ga_{0.32}In_{0.68}P bond interface structure for as-bonded and annealed samples. The images are recorded by aligning the Ga_{0.32}In_{0.68}P to $\langle 011 \rangle$ zone axis so the atomic columns are clearly visible. Note that the GaSb lattice is tilted by 3.6° relative to the Ga_{0.32}In_{0.68}P, due to an intentional offset of the GaSb wafer along the $\langle 011 \rangle$ zone axis.

Table I summarizes the bond resistances as well as the thickness of the amorphous interlayer determined from the *I-V* curves (Fig. 1) and STEM measurements in (Fig. 2). The indicated error for the bond resistances contains contributions from the resistance measurements of the substrates, the metal contacts, and the bond interfaces. By increasing the annealing temperature from 300 to 350 °C, the bond resistance decreases from 4.8 ± 1.4 to $3.3 \pm 1.3 \text{ m}\Omega \text{ cm}^2$. Otherwise, by further

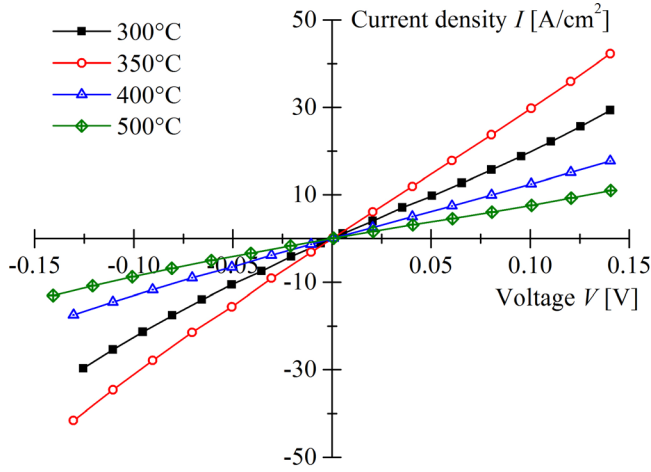


FIG. 1. I - V characteristics of n-GaSb/n-Ga_{0.32}In_{0.68}P wafer bonds annealed for 1 min at different temperatures.

increasing the temperature to 400 and 500 °C, the interfacial resistance rises again to 7.9 ± 1.7 and 12.8 ± 2.5 m Ω cm², respectively. The bond resistance of the as-bonded state is not shown because the metal contacts require at least 300 °C annealing to form an ohmic metal/semiconductor interface.

An amorphous interlayer is characteristic of the bond interfaces and appears in Fig. 2 as dark contrast between the two crystal lattices. In Table I, the quantitative measurements of the projected interlayer thicknesses from Figs. 2(a)–2(d) are summarized. The error bars result from variations in the interface thickness measured on the HAADF STEM images. The average interlayer thickness is 1.4 ± 0.2 nm in the as-bonded sample, and this value continuously decreases to thicknesses of 0.2 ± 0.2 nm after thermal annealing up to 500 °C. At this temperature, the crystalline lattices of GaSb and Ga_{0.32}In_{0.68}P partly interconnect with each other, with only few pockets of amorphous material remaining.

TABLE I. n-GaSb/n-GaInP bond resistance and amorphous interlayer thickness, dependent on the annealing temperature.

Annealing temperature (°C)	Bond resistance (m Ω cm ²)	Amorphous layer thickness (nm)
as-bonded	/	1.4 ± 0.2
300	4.8 ± 1.4	1.0 ± 0.3
350	3.3 ± 1.3	/
400	7.9 ± 1.7	0.6 ± 0.3
500	12.8 ± 2.5	0.2 ± 0.2

The STEM investigations revealed the formation of pores at the interface for annealing temperatures of 400 and 500 °C. To illustrate these observations, medium resolution HAADF STEM images are shown in Figs. 3(a)–3(d) for the different annealing conditions. The localized bright contrast, which is visible in the 400 °C annealed near-surface region of the GaSb crystal in Fig. 3(c), can be attributed to In enrichment and will be discussed below in the context of Fig. 4(c). Additionally, the slightly brighter contrast at the interface in Fig. 3(b) already indicates the onset of In enrichment in GaSb [compare Fig. 4(b)]. In Fig. 3(d), the formation of crystalline precipitates was observed in the GaSb crystal after an annealing at 500 °C.

Figure 4 shows an enlarged image of the precipitate that has formed in the GaSb crystal at 500 °C annealing. The focus of the HAADF STEM image was chosen to enhance the structure of the precipitate and to minimize the Moiré fringe contrast. The digital diffractograms (Fast Fourier Transformation of the lattice image intensities) in Fig. 4 show the relative reciprocal distances and orientations of the projected lattices for a region of the GaSb crystal with the precipitate (b) and without the precipitate (c).

By tuning the focusing conditions of the HAADF STEM image, the lattice pattern of the precipitate can be enhanced and used to identify its shape and structure. The atomic

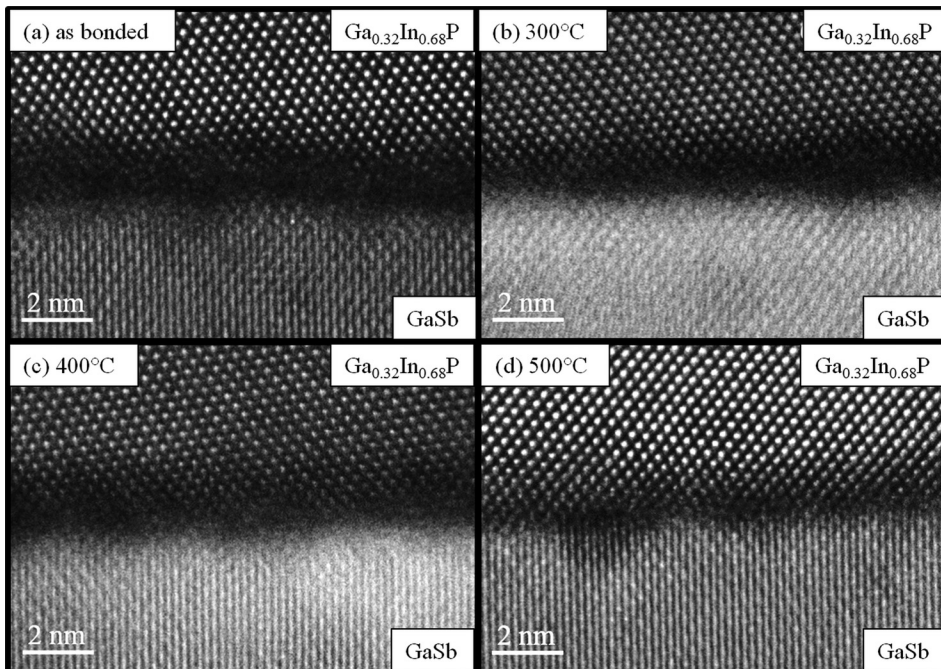


FIG. 2. High-resolution HAADF STEM images of n-GaSb/n-Ga_{0.32}In_{0.68}P bond interfaces viewed along the $\langle 011 \rangle$ Ga_{0.32}In_{0.68}P zone axis. (a) As-bonded interface and (b), (c), and (d) the interface after a 1 min annealing at 300, 400, and 500 °C, respectively. The slight misalignment between the crystal lattices leading to different contrasts of the atomic columns.

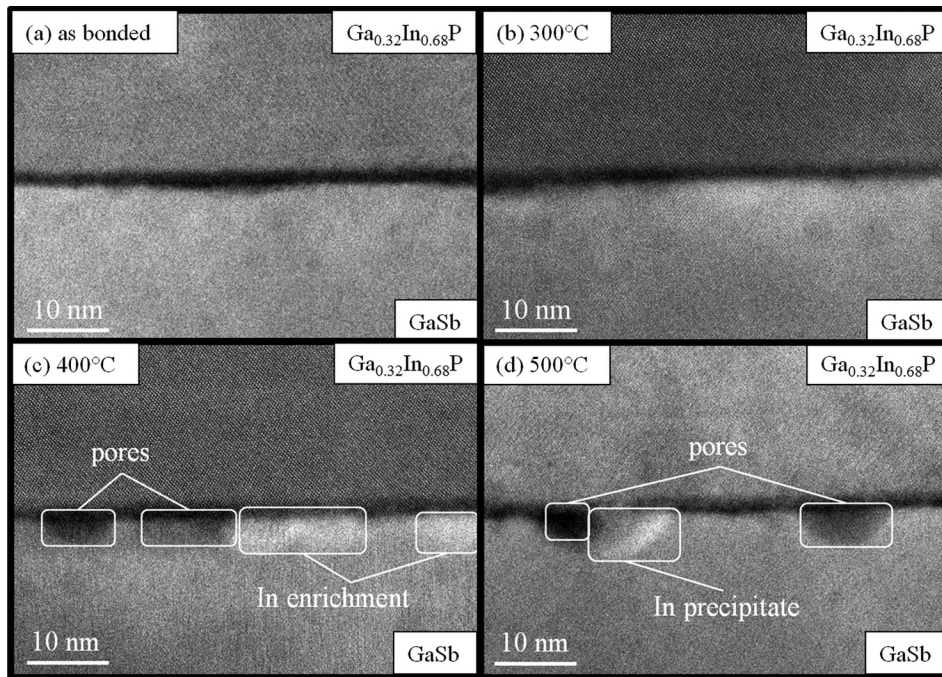


FIG. 3. Medium-resolution HAADF STEM images of the n-GaSb/n-Ga_{0.32}In_{0.68}P bond interfaces viewed along the $\langle 011 \rangle$ Ga_{0.32}In_{0.68}P zone axis. (a) As-bonded interface, (b), (c), and (d) the interface after a 1 min annealing at 300, 400, and 500 °C, respectively. The pores as well as the In enrichment and precipitate are highlighted in (c) and (d).

structure of the precipitate differs from the GaSb crystal. Based on the chemical analysis (see below) and digital diffractograms recorded from a GaSb region with/without the precipitate, the structure of the precipitate was identified as crystalline In which is known to possess the space group of $I4/mmm$ (139) and lattice constants of $a = b = 3.25 \text{ \AA}$ and $c = 4.95 \text{ \AA}$. The In is viewed from the $[100]$ direction. The GaSb reflections have been used as reference in the structure identification of the precipitate.

Figure 5 shows medium resolution HAADF STEM images and the corresponding chemical analysis of the interface structure extracted from high spatial resolution STEM EDXS spectrum imaging. The local concentrations of Ga, In, P, and Sb are plotted in atomic percentage vs. position for the

as-bonded state and annealed states. Sections of the interface regions are shown below each corresponding plot of the line profiles.

The analysis of the as-bonded state reveals that the inter-layer region is mainly composed of Ga, In, and P, while the onset of the Sb signal is slightly delayed relative to Ga [Fig. 5(a)]. This implies an enrichment of Ga in the amorphous layer. No significant signal of O was detected, confirming that the sputtering duration in the bond chamber was sufficient to remove native oxides. Starting at 300 °C, the In concentration increases in the near-surface region of GaSb, suggesting that diffusion takes place upon annealing [Fig. 5(b)]. When In enriches in GaSb, the Ga signal for this region is correspondingly lower. At 400 °C, the In peak is more pronounced compared to 300 °C [Fig. 5(c)]. At 500 °C, the In peak is again less pronounced [Fig. 5(d)] due to the concentration of In in precipitates [compare Fig. 4]. Accordingly, the highest In fraction is found in the line scans across the In precipitate in Fig. 5(e). At the same time, the atomic concentrations in a pore region [Fig. 5(f)] are similar to the results found for the sample without precipitates/pores [Fig. 5(d)]. No element is specifically depleted or enriched around the pore, indicating that the pore formation is not linked to the depletion of a certain element. Note that the X-ray signals measured by the EDX analysis result from a thin three-dimensional film, so a signal can be detected from atoms above or below the pore.

IV. DISCUSSION

The purpose of this study is to access the electrical properties of the interface between n-GaSb and n-Ga_{0.32}In_{0.68}P following surface-activated wafer bonding and their relationship with the microstructure, as well as with the effects of thermal annealing treatments. In the following, we discuss the relevant TEM measurements together with the corresponding electrical properties.

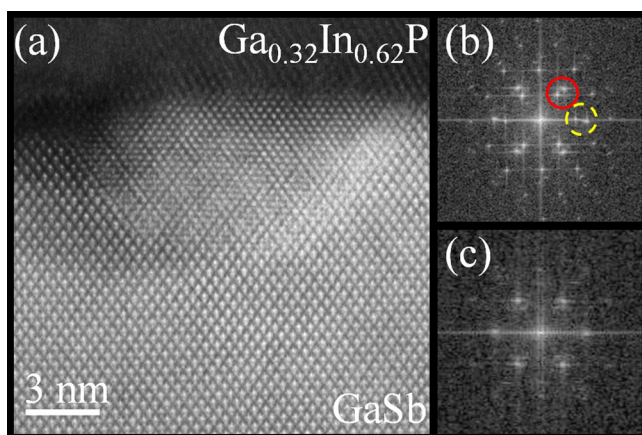


FIG. 4. (a) High-resolution HAADF STEM image of the precipitate visible in Fig. 3(d), observed after 500 °C annealing. Digital diffractograms recorded from the GaSb with precipitate are shown in (b) as well as from the GaSb without precipitate in (c). The lower point in the red circle in (b) correlates with the -111 reflex of GaSb and the upper point to the 011 reflex of In. The left point in the dotted yellow circle in (b) correlates with the 002 reflex of GaSb and the right point to the 002 reflex of In.

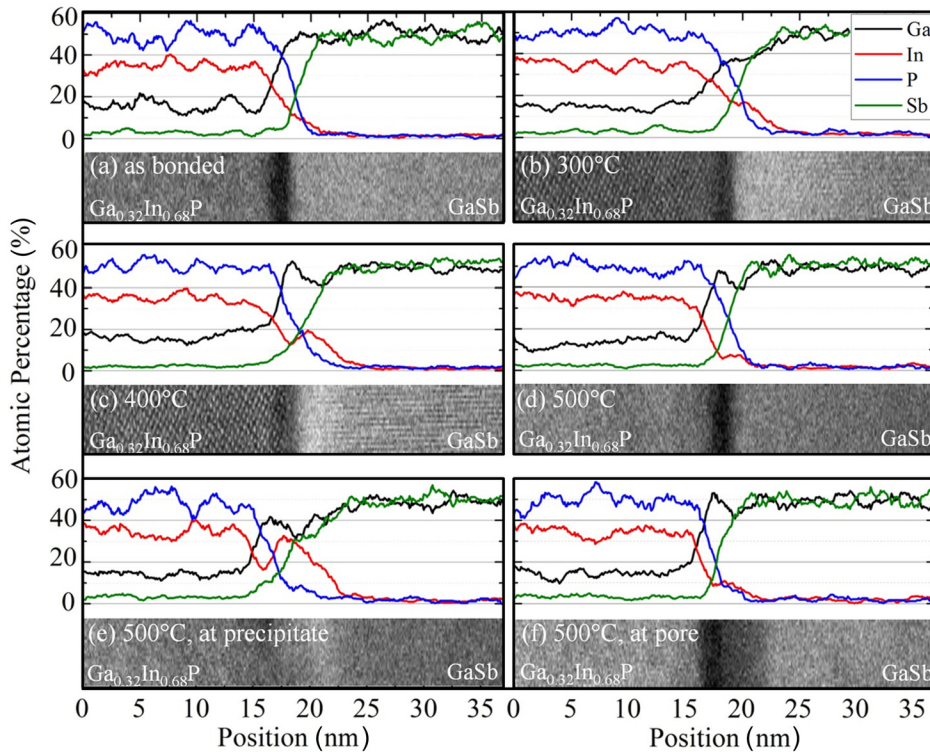


FIG. 5. Cross-sections of the n-GaSb/n-Ga_{0.32}In_{0.68}P bond interfaces in medium-resolution HAADF STEM image contrast together with the element distribution extracted from EDXS line scans. (a) As-bonded and (b), (c), and (d) annealed at 300, 400, and 500 °C, respectively. The images and the plots are correctly positioned with respect to each other and show identical interface regions. (e) and (f) show corresponding profiles for the precipitate and pore region of the sample annealed at 500 °C.

A. Microstructure of bond interfaces—as-bonded state

For the as-bonded state, the most important TEM observations are as follows:

- The existence of an ~ 1.4 nm thick amorphous interlayer between the crystalline GaSb and Ga_{0.32}In_{0.68}P [Fig. 2(a)].
- The presence of all elements constituting the semiconductor layers in this amorphous interlayer [Fig. 5(a)].
- The local enrichment of Ga at the bond interface [Fig. 5(a)].

The formation of an amorphous interlayer and the redistribution of elements (as compared to the nominal layer composition) are novel results for bond interfaces containing antimonides. The activation of the surfaces by sputtering with argon atoms and the subsequent bonding process are expected to lead to a complex interplay of defect generation, amorphization, and atom transport.

The initial amorphous layer thickness of ~ 1.4 nm is relatively thin, compared to published results for surface-activated wafer bonding. As-bonded interlayer thicknesses were reported to have thicknesses of ~ 8.3 nm for Si/Si bonds,¹⁴ ~ 2 – 3 nm for Si/GaAs bonds,²³ and ~ 7 nm for GaP/GaAs bonds,¹⁹ which were all activated with projectile energies of 1500 eV. Takagi *et al.* showed that the amorphous layer thickness is strongly influenced by the kinetic energy of the Ar atoms.¹³ So it can be concluded that the thin ~ 1.4 nm as-bonded GaSb/Ga_{0.32}In_{0.68}P interlayer is mainly a result of the low kinetic Ar atom energies of ~ 300 eV, which minimizes the sputtering-induced defect formation and amorphization.

The compositional change in the as-bonded interface compared to the nominal crystal compositions can be attributed to the wafer surface stoichiometries after sputtering. The bond interface shows Ga (group III) enrichment and

consequently group V deficiency. But the total group V always amounts to more than 40% of the atoms. So no metallic film is expected to form during the activation. Further details on sputtering-induced compositional changes in III-V semiconductors are given in a review by Malherbe, in which preferential sputtering is mainly explained by differences in the atomic masses and the surface-binding energies of the surface atoms.²⁴ GaSb showed no compositional changes after sputtering but InP and GaP showed in most studies a group III rich surface, which correlates with our results.²⁴

B. Microstructure of bond interfaces—Thermal annealing treatments

Thermal annealing of the heterojunctions led to the following microstructural characteristics:

- The continuous decrease in the average amorphous interlayer thickness with increasing annealing temperature, resulting from recrystallization during annealing [Figs. 2(a)–2(d)].
- At 300 °C, first signs for modified element distribution profiles, especially the enrichment of In in the near-interface region of GaSb [Fig. 5(b)].
- At 400 °C, enhanced enrichment of In in the GaSb near-interface region and formation of pores at the interface [Figs. 3(c) and 5(c)].
- At 500 °C, interfaces with largely interconnected crystal regions between the adjacent crystal layers and pockets of the remaining amorphous material [Fig. 2(d)], formation of larger pores, and further In-enrichment in GaSb, leading to the formation of crystalline In precipitates [Figs. 3(d), 4, and 5(e)].

During the annealing treatments, recrystallization of the amorphous interlayer and redistribution of elements occur in parallel. The recrystallization rate depends on the materials, on the pre-treatment, and on the chosen annealing condition. In our experiments, we found an almost full recrystallization after annealing at 500 °C with the chosen annealing conditions (1 min annealing in the forming gas atmosphere). As a comparison, the full recrystallization of an initially 11.3 nm thick amorphous interlayer at a GaAs/Si bond interface was obtained after annealing at 600 °C in air for 1 h.²⁵ Also the recrystallization of an initially 4 nm thick amorphous interlayer at a GaP/GaAs interface was completed after annealing in air for 1 h at 400 °C.¹⁹ Accordingly, the results for the GaSb/Ga_{0.32}In_{0.68}P bond are in line with previous experiments with other III-V semiconductors.

The In enrichment in the GaSb near-interface regions indicates the diffusion of In from Ga_{0.32}In_{0.68}P into the GaSb. When In diffuses into GaSb, strain will be induced within the crystal and potentially lead to crystal defects. The amount of In enriched in this region increases with temperature. The formation of In precipitates in connection with pores at 500 °C (Fig. 4) indicates its relationship with the diffusion and agglomeration of vacancy-type defects during annealing. The observed precipitates are identified as crystalline In. Two mechanisms are possible for the formation of the precipitates. First, In can agglomerate at a pore during the In diffusion at the annealing 500 °C. At this temperature, the In would be in a liquid phase (the melting point of In is 156.6 °C) that recrystallizes upon cooling down. Second, the solubility of In in GaSb is higher at 500 °C compared to room temperature.²⁶ Upon cooling down, this may lead to In oversaturation in the near-surface region of the GaSb and then result in phase separation.

The pore formation at 400 and 500 °C is a clear indication of the transport and the clustering of vacancy-type defects that occur in connection with the atomic diffusion. The average mass density at the bond interface is lower than in the bulk crystal, which is caused by the amorphous state of the interlayer as well as by the fact that the wafer surfaces were not atomically flat before bonding. The root mean square (RMS) roughness of the wafer surfaces before bonding is in the range of 0.5 nm and 0.2 nm for GaSb and Ga_{0.32}In_{0.68}P, respectively.¹² Upon annealing at temperatures >400 °C, the atoms in the amorphous layer rearrange and form a denser crystal lattice, whereas the initially vacant sites and roughness-induced open volume lead to formation of detectable pores. Additionally, argon that was implanted during the surface activation prior to bonding could contribute to the pore formation processes.

C. Electrical properties of the bond interfaces

The resistance of a bond interface depends mainly on the number of atomic bonds per area and potential barriers in the conduction bands resulting from different electron affinities of the materials and process-induced defects. These defects can potentially create defect states within the bandgap of the semiconductor that trap electrons.⁶ In this context, a relatively high doping of the bond layers is essential to achieve

ohmic bond resistances because this leads to an energetically high Fermi-level, reducing the effective interface barrier width and height in the conduction band. Still, the potential barriers often lead to non-ohmic bond resistances.^{7,8}

As can be seen in Fig. 1, ohmic behavior was observed for every annealing temperature, indicating that no barrier is present in the conduction band that would lead to diode-like characteristics. Furthermore, bond resistances in the range of few mΩ cm² are obtained for all annealing temperatures (compare Table I), which are in the range of the lowest reported bond resistances for surface-activated wafer bonding.^{12,18} According to the argumentation above, these low bond resistances are achieved by applying high doping concentrations in the bond layers (compare Sec. II) as well as by the small amount of amorphization and process-induced defect formation during bonding (compare Table I).

The increase in the annealing temperature from 300 to 350 °C leads to a decrease in the electrical bond resistance from 4.8 ± 1.4 to 3.3 ± 1.3 mΩcm². This enhancement of the electrical carrier transport can be correlated with the partial recrystallization of the amorphous layer, which is reflected in a reduction of the interlayer thickness from 1.4 ± 0.2 nm to 1.0 ± 0.3 nm. As a consequence, the probability of electron trapping is reduced. Along these lines, Essig *et al.* reported that dopants that became inactive during the sputtering process could be re-activated by thermal annealing.⁶ The decrease of the bond resistance with increasing annealing temperature due to interlayer recrystallization is also reported in earlier studies on n-GaAs/n-Si and p-GaP/n-GaAs bond interfaces.^{6,19}

Surprisingly, further increases of the annealing temperature to 400 and 500 °C result in higher resistances of 7.9 ± 1.7 and 12.8 ± 2.5 mΩ cm², respectively. This result is in contrast to expectations and earlier reports.^{6,19} The advanced recrystallization leads to further thinning of the amorphous interlayer to 0.6 ± 0.3 nm (for 400 °C) and 0.2 ± 0.2 nm (for 500 °C). This should result in a decreased bond resistance due to the reasons stated above. Thus, it can be concluded that the effect of recrystallization is overcompensated by other mechanisms at the bond interface for annealing temperatures >400 °C. The resistance increase can be correlated with the formation of new interfacial defects, which were detected in the TEM analysis, namely, the formation of pores and the In enrichment in GaSb, which leads to In precipitation at 500 °C. The observed pores reduce the effective number of atomic bonds per interface unit area that are contributing to the current flow, and consequently, the bond resistance in Ωcm² increases linearly with the reduction of the bonded area.¹² Additionally, the temperature-induced interfacial defects can potentially lower the conductivity by creating new defect states in which electrons are trapped, thus reducing the amount of electrons that can conduct between the n-GaSb and n-Ga_{0.32}In_{0.68}P layers.⁶ It should be noted that the In precipitates might increase the conductivity if an additional low resistance current path between the two semiconductors is created. Nevertheless, this is not the case, as it can be seen in Fig. 3(d) that the precipitate is located completely in the crystalline GaSb, adjacent to the still remaining amorphous bond interlayer.

V. CONCLUSION

Advanced methods of high-resolution STEM combined with EDXS have been applied to assess the microstructure of n-GaSb/n-Ga_{0.32}In_{0.68}P bond interfaces upon thermal annealing up to 500 °C and its relationship to the electrical properties, characterized by *IV* curves. An amorphous interlayer with ~1.4 nm thickness is found in the as-bonded interface, which continuously recrystallizes upon annealing, forming a largely crystalline interface at 500 °C.

These low interlayer thicknesses correlate with low ohmic bond resistances of few mΩ cm² for every annealing temperature. When the annealing temperature is increased, two opposing effects could be identified in the microstructure, which mainly determines the bond resistance. The stronger recrystallization of interfacial defects with increasing temperature reflects the decrease in the bond resistance from ~4.8 mΩ cm² for an annealing at 300 °C to ~3.3 mΩ cm² at 350 °C. At 400 °C annealing, the effect of recrystallization is overcompensated by the generation of new interfacial defects. These are mainly the formation of pores as well as In enrichment in the near-surface region of GaSb. The outcome is an increased bond resistance of ~7.9 mΩ cm² after 400 °C annealing. At 500 °C, the formation of larger pores is observed and also In diffusion into GaSb continues, leading to the creation of crystalline In precipitates within the GaSb. Accordingly, the highest bond resistance of ~12.8 mΩ cm² was obtained for annealing at 500 °C.

The presented analysis of n-GaSb/n-Ga_{0.32}In_{0.68}P bond microstructures including the depicted effects of thermal annealing and its correlation with the bond resistance is of general value for the design and optimization of heterojunctions based on III-V materials that require high electrical conductivity. Utilizing the investigated n-GaSb/n-Ga_{0.32}In_{0.68}P wafer bond after an annealing at 350 °C, a novel four-junction solar cell based on Ga_{0.50}In_{0.50}P/GaAs/Ga_{0.79}In_{0.21}As//GaSb has been successfully fabricated with an efficiency of 29.1% under concentration.³

ACKNOWLEDGMENTS

The authors would like to thank R. Freitas for processing the wafer bonds for the conductivity measurements and D. Meertens and W. Sybertz for assistance in the TEM specimen preparation. F. Predan gratefully acknowledges the funding

support for his Ph.D. work by the German Federal Environmental Foundation, DBU (Contract No. 20014/344). This work was partly funded by the German BMWi through the project HekMod4 (Contract No. 0325750).

- ¹I. Vurgaftman, J. R. Meyer, and L. R. Ram-Mohan, *J. Appl. Phys.* **89**(11), 5815–5875 (2001).
- ²M. A. Green, K. Emery, Y. Hishikawa, W. Warta, and E. D. Dunlop, *Prog. Photovoltaics: Res. Appl.* **24**(7), 905–913 (2016).
- ³F. Dimroth, T. N. D. Tibbits, M. Niemeyer, F. Predan, P. Beutel, C. Karcher, E. Oliva, G. Siefert, D. Lackner, P. Fuß-Kailuweit, A. W. Bett, R. Krause, C. Drazek, E. Guiot, J. Wasselin, A. Tauzin, and T. Signamarcheix, *IEEE J. Photovoltaics* **6**(1), 343–349 (2016).
- ⁴T. Suga, Y. Takahashi, H. Takagi, B. Gibbesch, and G. Ellsner, *Acta Metall. Mater.* **40**, S133–S137 (1992).
- ⁵O. Moutanabbir and U. Gösele, *Annu. Rev. Mater. Res.* **40**, 469–500 (2010).
- ⁶S. Essig and F. Dimroth, *ECS J. Solid State Sci. Technol.* **2**(9), Q178–Q181 (2013).
- ⁷S. Essig, O. Moutanabbir, A. Wekkeli, H. Nahme, E. Oliva, A. W. Bett, and F. Dimroth, *J. Appl. Phys.* **113**(20), 203512–203516 (2013).
- ⁸M. M. R. Howlader, T. Watanabe, and T. Suga, *J. Vac. Sci. Technol., B: Microelectron. Nanometer Struct.* **19**(6), 2114–2115 (2001).
- ⁹M. M. R. Howlader, T. Watanabe, and T. Suga, *J. Appl. Phys.* **91**(5), 3062–3066 (2002).
- ¹⁰S. Uchida, T. Watanabe, H. Yoshida, and H. Yang, *Appl. Phys. Express* **7**(11), 112301 (2014).
- ¹¹F. Predan, D. Reinwald, V. Klinger, and F. Dimroth, *Appl. Surf. Sci.* **353**, 1203–1207 (2015).
- ¹²F. Predan, D. Reinwand, R. Cariou, M. Niemeyer, and F. Dimroth, *J. Vac. Sci. Technol., A* **34**(3), 031103 (2016).
- ¹³H. Takagi, M. Ryutaro, N. Hosoda, and T. Suga, *Jpn. J. Appl. Phys.* **38**(3A), 1589–1594 (1999).
- ¹⁴M. M. R. Howlader and F. Zhang, *Thin Solid Films* **519**(2), 804–808 (2010).
- ¹⁵T. R. Chung, L. Yang, N. Hosoda, and T. Suga, *Nucl. Instrum. Methods Phys. Res. B* **121**(1–4), 203–206 (1997).
- ¹⁶D. Häussler, L. Houben, S. Essig, M. Kurttepel, F. Dimroth, R. E. Dunin-Borkowski, and W. Jäger, *Ultramicroscopy* **134**, 55–61 (2013).
- ¹⁷K. Tanabe, K. Watanabe, and Y. Arakawa, *Sci. Rep.* **2**, 349 (2012).
- ¹⁸S. Uchida, T. Watanabe, H. Yoshida, T. Tange, M. Arimochi, M. Ikeda, D. Pan, H. Wei, J. Lian, L. Shulong, and Y. Hui, *Appl. Phys. Express* **7**(11), 112301 (2014).
- ¹⁹M. M. R. Howlader, T. Suga, F. Zhang, T. H. Lee, and M. J. Kim, *Electrochem. Solid-State Lett.* **13**(3), H61–H65 (2010).
- ²⁰M. M. R. Howlader, P. R. Selvaganapathy, and M. J. Deen, *IEEE J. Sel. Top. Quantum Electron.* **17**(3), 689–703 (2011).
- ²¹S. Saied, J. L. Sullivan, and R. K. Fitch, *Vacuum* **38**(2), 111–115 (1988).
- ²²G. Cliff and G. W. Lorimer, *J. Microsc.* **103**(2), 203–207 (1975).
- ²³T. R. Chung, L. Yang, N. Hosoda, and T. Suga, *Nucl. Instrum. Methods Phys. Res. B* **121**, 203–206 (1997).
- ²⁴J. B. Malherbe, *Crit. Rev. Solid State Mater. Sci.* **19**(3), 129–195 (1994).
- ²⁵T. Yu, M. R. Howlader, F. Zhang, and M. Bakr, *ECS Trans.* **35**(2), 3–10 (2011).
- ²⁶G. Dhanaraj, *Springer Handbook of Crystal Growth* (Springer Verlag, Heidelberg, Germany, 2010).